

Dendritic flux penetration in Pb films with a periodic array of antidots

M. Menghini, R. J. Wijngaarden

Department of Physics and Astronomy,

Faculty of Sciences, Vrije Universiteit,

De Boelelaan 1081, 1081HV Amsterdam, The Netherlands

A. V. Silhanek*, S. Raedts, and V. V. Moshchalkov

Nanoscale Superconductivity and Magnetism Group,

Laboratory for Solid State Physics and Magnetism K. U. Leuven

Celestijnenlaan 200 D, B-3001 Leuven, Belgium

(Dated: March 23, 2022)

Abstract

We explore the flux-jump regime in type-II Pb thin films with a periodic array of antidots by means of magneto-optical measurements. A direct visualization of the magnetic flux distribution allows to identify a rich morphology of flux penetration patterns. We determine the phase boundary $H^*(T)$ between dendritic penetration at low temperatures and a smooth flux invasion at high temperatures and fields. For the whole range of fields and temperatures studied, guided vortex motion along the principal axes of the square pinning array is clearly observed. In particular, the branching process of the dendrite expansion is fully governed by the underlying pinning topology. A comparative study between macroscopic techniques and direct local visualization shed light onto the puzzling T - and H -independent magnetic response observed at low temperatures and fields. Finally, we find that the distribution of avalanche sizes at low temperatures can be described by a power law with exponent $\tau \sim 0.9(1)$.

* present address: MST-NHMFL, MS E536, Los Alamos National Laboratory, Los Alamos, NM 87544, USA.

I. INTRODUCTION

Flux penetration in a type-II superconductor in the mixed state is usually described by the Bean critical state model. In this approximation it is assumed that a balance between the pinning force and the external magnetic pressure leads to a constant flux gradient.¹ Similarly to a sand pile, this vortex distribution is metastable and therefore it is bound to decay to a lower energy configuration. The dynamic evolution towards the equilibrium state is generally described as flux creep where thermal or quantum fluctuations are needed to overcome a current dependent pinning barrier $U(j)$.² If this process takes place under isothermal conditions the creep is logarithmic in time and the field penetration is smooth with a flat flux front.^{3,4} In contrast, if the process is perfectly adiabatic, the heat dissipation δQ produced by the vortex motion will give rise to a local increase of the temperature $\delta T = \delta Q/C$, where C is the specific heat of the superconducting material. Since typically $dJ_c/dT < 0$, this local rise of temperature implies a reduction of the critical current which in turn promotes further vortex motion thus yielding a vortex avalanche. In this scenario, the field penetration is abrupt, giving rise to jumps in the magnetization, and develops much faster than the creep relaxation process. These avalanches (or flux-jumps) occur at low temperatures where critical currents are high and the specific heat is small thus severely undermining the potential technological applications of superconducting materials.⁵

In most cases, flux penetration experiments are performed in thin superconducting materials of slab geometry exposed to a field perpendicular to the sample plane. It has been observed for many samples that in this configuration the field penetrates via highly branched expansions giving rise to a dendritic pattern of flux channels.^{6,7} Theoretical studies as well as numerical simulations^{7,8}, have reproduced the observed flux penetration patterns in thin films giving support to a thermo-magnetic origin for these type of instabilities.

On the other hand, the influence of the pinning landscape on the morphology and local characteristics of dendritic flux penetration has not been yet fully addressed. A model system to investigate this effect can be realized by tailoring a periodic pinning array in superconducting samples. Vortex avalanches have been previously detected^{9,10,11,12} in thin films with periodic pinning arrays. Global magnetization measurements^{10,11,12} in samples with arrays of antidots have shown that the region in the $H - T$ phase diagram dominated by flux-jumps is more extended as compared to the case of plain films. Besides that, com-

measurability of flux-jumps with the matching field of the pinning lattice and invariance of the magnetization and flux-jump size distribution at low temperatures and fields were observed. Moreover, magneto-optical (MO) imaging⁹ in Nb patterned films has shown that vortex avalanches along the principal directions of the pinning lattice take place in zero-field cooling (ZFC) experiments. From the theoretical point of view, Aranson *et al.*⁸ have shown that a periodic spatial modulation of the critical current gives rise to a branching pattern of local temperature following the symmetry of the underlying pinning array.

In this work we study the flux-jump regime in Pb thin films with periodic pinning by means of MO. In order to separate and clearly identify the effects of the engineered pinning potential similar experiments were performed on plain Pb films. The characteristics of the samples and the MO technique are described in the following section. Subsequently, the different types of flux penetration in ZFC experiments at different temperatures are described. Additionally, phase boundary separating dendritic from smooth penetration was determined. Finally, we present an analysis of the evolution of dendrites with field and we study the avalanche size distribution as a function of temperature.

II. SAMPLES AND EXPERIMENTAL PROCEDURE

The experiments were conducted on Pb thin films with a square array of antidots. The dimensions and critical temperature for each sample are summarized in Table I. In all patterned samples the square antidot array consists of square holes with lateral dimension $b = 0.8 \mu\text{m}$ and period $d = 1.5 \mu\text{m}$ which corresponds to a first matching field $\mu_0 H_1 = 0.92 \text{ mT}$. Simultaneously with each patterned film we deposited also an unpatterned reference film on a SiO_2 substrate which allows us to perform a direct comparison in order to ascertain the effects of the pinning array (see Table I). Due to geometrical characteristics these Pb thin films are type-II superconductors.^{13,14} From the temperature dependence of the upper critical field $H_{c2}(T)$ of the plain films we have estimated a superconducting coherence length $\xi(0) = 33 \pm 3 \text{ nm}$. A more detailed description of the sample preparation can be found in Ref.[15].

The local magnetic induction, B , just above the surface of the sample was measured using a magneto-optical image lock-in amplifier technique as described in Ref.[16]. The magnetic induction was sensed using an indicator with in-plane magnetization and large Faraday effect

TABLE I: Lateral dimensions (w_1 and w_2), thickness (t), and critical temperatures (T_c) for all the films studied. AD indicates a square array of antidots and PF a plain film.

Sample	w_1 (mm)	w_2 (mm)	t (nm)	T_c (K)
AD75	1.6	2.9	75	7.21
AD65	2.3	2.5	65	7.21
AD15	1.9	2.0	13.5	7.10
PF15	2.2	3.1	13.5	7.10

mounted on top of the sample. The sample together with the indicator were mounted in a specially designed cryogenic polarization microscope. The experiments were performed in a commercial Oxford Instruments 7 T vector magnet system.

III. RESULTS AND DISCUSSION

A. Dendrite morphology

Magneto-optical imaging of Pb films with a square array of antidots shows a rich variety of magnetic flux penetration in ZFC experiments as a function of temperature. Fig. 1 summarizes the different morphologies of flux penetration observed in these samples. The brighter regions correspond to high magnetic fields while the dark ones indicate zero field. In the bottom part of Figs. 1 (a)-(d) magnetic domains from the magneto optical garnet show up as a saw-tooth-like boundary between regions with different contrast. These domains do not seem to influence the flux pattern inside the sample and are irrelevant for the discussion below. At low T and H finger-like dendrites elongated in the direction perpendicular to the sample's border are formed (Fig. 1(a)). As the temperature increases to 5.5 K the dendrites become considerably larger and more branched (see Fig. 1(b)). In the range, $5.5 < T \leq 6$ K, the magnetic field first penetrates smoothly up to approximately $1/4$ of the sample width ($\mu_0 H \sim 1.5$ mT) and then suddenly a highly branched dendrite is formed. An example of this behavior, also predicted theoretically⁸, is shown in Fig. 1(c). In the present sample we found highly branched (tree-like) dendrites for applied fields up to 3 mT, for higher fields

the penetration becomes uniform. It is noteworthy that in the finger-like regime the maximum length of dendrites is limited by the half width of the sample whereas in the region of highly-branched or tree-like dendrites, vortices can extend much further into the sample. Finally, for $T > 6$ K a smooth flux penetration is observed (Fig. 1(d)) in the whole range of fields investigated and a Bean-like pattern develops.

Within the regime dominated by avalanches it is found that the main core of the dendrites and their ramifications are oriented along the principal directions of the square array of antidots. However, the influence of the underlying periodic pinning array is not constrained to the flux-jump regime but can also be seen in the smooth Bean-like penetration pattern. Indeed, a closer look at the flux front for $T > 6$ K shows clear streaks aligned with the pinning array as a result of preferential or guided motion of vortices.¹⁷ This result is consistent with previous reports in low temperature as well as high temperature superconductor thin films with periodic pinning.^{17,18,19} On the other hand, it has been theoretically shown that, in samples with random disorder, during the initial ramping of the field hot magnetic filaments propagate from the border of the sample. This, could eventually also lead to streaks in the field penetration.⁸ However, since we have observed a filamentary penetration only in the patterned sample and not in the plain film, we can rule out this possibility and attribute the observed effect to the periodic pinning potential.

The influence of the square lattice of antidots on the flux penetration becomes more evident when comparing the previous results with those obtained in Pb plain films (PF) (Figs. 1 (e) and (f)). In this case, ZFC MO experiments show that the vortex avalanche regime is constrained to a smaller region of the $H - T$ phase diagram (see Fig. 2(b)). Besides that, as can be clearly seen in the flux patterns formed at low temperatures (Fig. 1(e)), the morphology of the dendrites is quite different from the one described above for antidot samples. In PF we observe that the magnetic field bursts in highly disordered dendrites with no particular orientation (other than the average imposed by the screening currents) and with no characteristic size. These features are similar to those previously reported for Nb and MgB₂ plain films.^{6,7} Finally, a smooth penetration is found at high temperatures and fields, as in the case of the patterned sample.

In all cases, we have observed that the dendrites develop rather abruptly, $v > 10$ m/s, according to the limit imposed by our experimental temporal resolution. Previously, it was shown that this velocity can indeed be much higher.²⁰ Besides this, dendrites nucleate at

the edge of the sample in random positions which do not reproduce if the experiment is repeated. This indicates that their appearance is an intrinsic property of the system rather than due to imperfections in the sample's border.²¹

B. Phase diagram

The transition line $H^*(T)$ from avalanche to smooth flux penetration regimes in Pb films with antidots was previously determined from dc-magnetization and ac-susceptibility measurements.^{11,12} In the former case, the vortex avalanche regime manifests itself as a jumpy response of the magnetization, whereas in ac-susceptibility measurements the signature of the transition between the different flux penetration regimes is a local paramagnetic reentrance in the ac-screening.¹²

In Fig. 2 we plot the $H^*(T)$ lines previously reported using ac-susceptibility together with the those determined by ZFC MO measurements. Fig. 2(a) shows the phase boundary obtained for samples with the same antidot array and a slightly (15%) different thickness. The remarkable agreement between these two type of experiments reinforces the interpretation of the reentrance in the ac-screening as the onset of dendritic vortex avalanches. For comparison, the boundary lines corresponding to samples with and without antidots are shown in Fig. 2(b). In this case both samples were deposited simultaneously and have the same thickness. The $H^*(T)$ line for the non-patterned sample was determined by MO imaging whereas the boundary for the antidot sample was obtained by ac-susceptibility and is the same as already shown in Ref.[12]. In Fig. 2(b) we can clearly see that the flux-jump regime covers a larger portion of the phase diagram for the patterned sample than for the plain film, in agreement with previous reports.^{11,12}

Hébert *et al.*¹¹ proposed that the larger extension of the avalanche regime in presence of antidots can be related to the formation of a multi-terrace critical state^{22,23} in this kind of samples. Within this model, the main precursor of avalanches is the abrupt local change $\delta B(x)$ in between terraces of constant B . However, the direct observation of vortex dendrites indicates that this scenario is not appropriate to describe the observed extension of the flux-jump regime.

C. Dendrite field evolution

In order to gain more insight into the dynamics of the avalanches we studied the magnetic induction profile inside the dendrites in ZFC experiments where the external field is increased in discrete steps. In Fig. 3(a) a 3D image of the field distribution near one edge of the sample with antidots at $T = 4$ K and $\mu_0 H = 1.8$ mT is given. Fig. 3(b) shows the magnetic field profile inside the dendrite along the line indicated by A-A' in Fig. 3(a) for different applied fields. During the experiment the external field was increased in steps of $\delta H = 0.2$ mT but in Fig. 3(b) for clarity we show only curves at $\delta H = 0.4$ mT. In both figures a maximum of B at the edge of the sample is clearly seen as expected for a thin film in a transverse magnetic field due to demagnetization effects.

In general, we observe that once a dendrite develops, its *shape* remains practically unchanged as the field is further increased. Additionally, as can be seen in Fig. 3(b), the internal field B along a dendrite (A-A' line) increases as one moves from the edge towards the center of the sample. Moreover, the magnitude of the magnetic induction inside the dendrite can be even higher than the field at the edge of the sample. After a dendrite has formed, the initial deficiency of vortices near the edge of the sample is progressively filled by new avalanches as the external field is ramped up (see for example the field profiles for $H \geq 2.4$ mT in Fig. 3(b)). As already pointed out by Barkov *et al.*,²⁴ the initial inhomogeneous distribution of vortices along the dendrites can be attributed to the field induced by the screening currents that flow around the dendrite. The field lines associated with these currents are more dense near the front of the dendrite giving rise to higher local field at that point.

Before the avalanche event occurs, the field penetrates following a Bean-like profile ($H < 1.2$ mT in Fig. 3(b)). Interestingly, right after the avalanche develops, this slope relaxes, as expected for a field-cooling process, and for higher applied fields it recovers again. A similar effect was previously observed in Nb films.²⁵

The evolution of the shape of the dendrites in their transverse direction is shown in Fig. 3(c). These profiles are calculated along the line defined by B-B' in Fig. 3(a) where no side branches of the dendrites are crossed. For the sake of clarity the curves have been displaced vertically. Naturally, the appearance of new peaks as the field is increased corresponds to the formation of new dendrites. The average width of the core of the dendrites is

$w \sim 45\mu\text{m} \sim 30d$, thus involving many unit cells of the periodic pinning array. From this sequence of profiles it can be seen that *the width of the peaks does not change with field*. Also, no clear temperature dependence of the dendrite width has been observed.

D. Avalanche size distribution

Since MO imaging maps the spatial distribution of B inside the sample we can calculate not only the total magnetic flux involved in all avalanches but also the number of vortices involved in a single avalanche. In order to do that, we subtract two consecutive MO images such that only relative changes are recorded. Then we identify all avalanches that took place at a given change in magnetic field and calculate the area, A_i , and the magnetic flux, Φ_i involved in each single avalanche event. Also we sum all the events for a given field step. The resulting values $\Phi_T = \sum \Phi_i$ and $A_T = \sum A_i$ for all fields and at three different temperatures are shown in Fig. 4(a) and (b).

Since avalanches stop at a temperature dependent field $H^*(T)$ the analysis is significant up to a certain field that is smaller for higher temperatures as can be seen from Fig. 2. It is interesting to note that the avalanches start at a field $\mu_0 H \sim 0.7$ mT (see vertical dotted line in Fig. 4). This minimum magnetic field is independent of the used magnetic field step and temperature, thus indicating that it is a characteristic field of these type of instabilities. The existence of a minimum field for the development of the first avalanche or the first flux-jump, was predicted theoretically and observed in many experiments.²⁶ This feature was also found in recent numerical and analytical studies of instabilities of field penetration in thin films with random disorder.⁸

In Fig. 4(a) we observe a noisy behavior of Φ_T as H increases, in agreement with the observed jumpy magnetization.¹¹ Fig. 4(b) shows the area of the sample invaded by vortex avalanches for each step of $\mu_0 H$. Within the inherent noise due to avalanche behavior, the data in both figures collapse onto a single curve for all temperatures. From the data shown in these figures, we can roughly estimate the internal field increment δB at each external $\delta H = 0.4$ mT step. Indeed, from Fig. 4(a) we have $\Phi_T \sim 8 \cdot 10^{-10}$ Tm² and from Fig. 4(b), $A_T \sim 0.3$ mm², thus we obtain $\delta B = \Phi_T \times A_T \sim 2.6$ mT within the avalanches which is approximately 6 times larger than the change in the applied field. This difference, of course, is a consequence of the inhomogeneous distribution of vortices in the avalanche

regime leading to a strongly focussed flux penetration. Averaging over the whole sample gives $\delta B \sim \delta H$. The observation of a δB independent of H and T is consistent with the previously reported temperature independent flux-jumps in similar samples.^{11,12}

We have pointed out in Section III.A that dendrites at $T = 5.5$ K exhibit more branching than at lower temperatures (see Fig.1). This effect becomes evident in Fig.4(c) where the average avalanche size, $\langle \Phi \rangle$, is plotted as a function of $\mu_0 H$ for the same three temperatures as in (a) and (b). The average is calculated for each applied field as $\langle \Phi \rangle = \sum \Phi_i / N$ where N is the number of avalanches that takes place at that field. From the figure it is evident that at $T = 3.5$ K and 4.5 K the average avalanche sizes are similar whereas at $T = 5.5$ K there is a substantial increase in $\langle \Phi \rangle$. This result is consistent with a scenario where finger-like dendrites of a well-defined size dominate at low T whereas large, highly branched tree-like dendrites, with no characteristic size, dominate at high T . The present analysis of avalanche sizes shows that even though the average size of the dendrites depends on temperature, the total flux involved in all avalanches remains approximately constant.

In addition to the analysis of magnetic flux and area of avalanches presented above, similar to a bulk magnetization measurement, the identification of each avalanche event allows us to analyze the *distribution* of individual avalanche sizes in the whole dendritic penetration regime. Presently, there is controversy on whether the critical state in superconductors is a self organized critical (SOC) system or not.²⁷ In the first case the size distribution will be described by a power law since avalanches of all sizes are expected. In our samples we find that the avalanche size distribution (we define the size by the total amount of moved flux) is consistent with power law behavior for $T < 5.5$ K (see Fig.5). However, at large avalanche sizes the data departs from a linear behavior in the log-log scale. This is due to a finite size effect since the length of the dendrites is limited by the size of the sample²⁸. Clearly we observe power-law behavior over one and a half decade consistently with SOC behavior. At $T = 5.5$ K a reliable fitting is not possible since the small amount of avalanches results in a very poor statistics (in this case there are of the order of 80 avalanches while at 4.5 K the number is 200). The power-law exponent extracted from the fitting of the data at low temperatures is $\tau \sim 0.9(1)$. A similar value ($\tau = 1.09$) has been obtained recently by Radovan and Zieve²⁷ in Pb plain films by analyzing the size of the magnetization jumps using local Hall probe measurements. For $\text{YBa}_2\text{Cu}_3\text{O}_7$ Aegerter *et al.*²⁹ found a slightly larger value $\tau = 1.29(2)$.

IV. CONCLUSIONS

We have studied magnetic flux penetration in Pb thin films with antidots by means of MO imaging. At low temperatures and fields the penetration is dominated by vortex avalanches while at higher T and H a rather smooth and flat flux front is observed. We have found that the avalanches develop in the form of dendrites similarly to previous observations in Nb films with a periodic antidot array. The morphology of the dendrites changes with temperature, from finger-like at low T to tree-like at high T . For all $H - T$ we observe that the vortex motion is guided by the pinning potential generated by the antidots. In general, new dendrites are formed far from old dendrites, in regions where previously no invasion of vortices has taken place, indicating that they interact repulsively. This occurs until there is no room for a new dendrite. As a consequence, the emergence of new dendrites leads to a more uniform magnetic field distribution.

The boundary between dendritic and smooth penetration as determined by MO imaging is in a very good agreement with the results obtained from ac-susceptibility measurements in similar samples, see Fig. 2. We have also corroborated that in the film with antidots the vortex avalanche regime is extended to higher temperatures and fields as compared to the case of unpatterned films. The detection of dendritic penetration in the flux-jump regime shows that the proposed model^{11,12} of multi-terrace formation for flux penetration is not applicable at low temperatures for Pb films with antidots. Magnetic field profiles inside the dendrites indicate that the field at the tip of the dendrite is of the order or even higher than the field at the edge of the sample. This is due to the high field induced by the screening currents, which make a hairpin bend at the end of the dendrite. A relaxation of the magnetic field slope at the edge of the sample due to the avalanche is observed.

Avalanche size distribution analysis shows that the sum of the flux over all avalanches remains constant with temperature. This accounts for the observed temperature independent magnetization at low H and T . However, we find that the average size of the dendrites depends on temperature. Thus, a detailed knowledge of the morphology of avalanches is necessary for a complete description of flux penetration in these superconducting thin films. Besides this global analysis of vortex avalanches we study the size distribution of individual avalanches taking profit of the local character of our technique. We find that the size distribution of individual avalanches is consistent with a power law behavior over more than

a decade of avalanche sizes at low temperatures. However, the absence of finite size scaling analysis²⁸ does not allow to make a definite conclusion on whether the system is SOC or not.

Recently, it was demonstrated that the coupling between nonlocal flux diffusion with local thermal diffusion can account for dendritic penetration in plain films. We believe that a similar analysis for the case of samples with periodic pinning will be very helpful for a complete understanding of magnetic flux instabilities in superconducting samples.

Acknowledgments

We would like to thank R. Jonckheere for fabrication of the resist patterns. This work was supported by the Belgian Interuniversity Attraction Poles (IUAP), Research Fund K.U.Leuven GOA/2004/02, the Fund for Scientific Research Flanders (FWO) and ESF “VORTEX” program and by FOM (Stichting voor Fundamenteel Onderzoek der Materie) which is financially supported by NWO (Nederlandse Organisatie voor Wetenschappelijk Onderzoek).

-
- ¹ C. P. Bean, Phys. Rev. Lett. **8**, 250 (1962)
 - ² P. W. Anderson, Phys. Rev. Lett. **9**, 309 (1962)
 - ³ A. Forkl, H. -U. Habermeier, R. Knorpp, H. Theuss, and H. Kronmüller, Physica C **211**, 121 (1993).
 - ⁴ M. R. Koblishka, Th. Schuster, B. Ludescher, and H. Kronmüller, Physica C **190**, 557 (1992).
 - ⁵ R. G. Mints and A. L. Rakhmanov, Phys. Mod. Phys. **53**, 551 (1981).
 - ⁶ C. A. Durán, P. L. Gammel, R. E. Miller, and D. J. Bishop, Phys. Rev. B **52**, 75 (1995).
 - ⁷ T. H. Johansen, M. Baziljevich, D. V. Shantsev, P. E. Goa, Y. M. Galperin, W. N. Kang, H. J. Kim, E. M. Choi, M. S. Kim, S. I. Lee, Supercond. Sci. Tech. **14**, 726 (2001).
 - ⁸ I. Aranson, A. Gurevich, and V. Vinokur, Phys. Rev. Lett. **87**, 067003 (2001), I. S. Aranson, A. Gurevich, M. S. Welling, R. J. Wijngaarden, V. K. Vlasko-Vlasov, V. M. Vinokur, and U. Welp, submitted for publication (2004).
 - ⁹ V. Vlasko-Vlasov, U. Welp, V. Metlushko, G. W. Crabtree, Physica C **341** 1281 (2000).

- ¹⁰ A. Terentiev, D. B. Watkins, L. E. De Long, L. D. Cooley, D. J. Morgan, and J. B. Ketterson, Phys. Rev. B **61**, R9249 (2000).
- ¹¹ S. Hébert, L. Van Look, L. Weckhuysen, and V. V. Moshchalkov, Phys. Rev. B **67**, 224510 (2003).
- ¹² A. V. Silhanek, S. Raedts, and V. V. Moshchalkov, to be published in Phys. Rev. B.
- ¹³ G. J. Dolan and J. Silcox, Phys. Rev. Lett. **30**, 603 (1973).
- ¹⁴ W. Rodewald, Phys. Lett. **55A**, 135 (1975).
- ¹⁵ S. Raedts, A. V. Silhanek, M. J. Van Bael, and V. V. Moshchalkov, Physica C **404**, 298 (2004).
- ¹⁶ R. J. Wijngaarden, K. Heeck, M. Welling, R. Limburg, M. Pannetier, K. van Zetten, V. L. Roorda, A. R. Voorwinden, Rev. Sci. Instrum. **72**, 2661 (2001).
- ¹⁷ M. Pannetier, R. J. Wijngaarden, I. Fløan, J. Rector, B. Dam, R. Griessen, P. Lahl, and R. Wördenweber, Phys. Rev. B **67**, 212501 (2003).
- ¹⁸ M.S. Welling, R.J. Wijngaarden, C.M. Aegerter, R. Wördenweber and P. Lahl, Physica C **404**, 410 (2004).
- ¹⁹ R. Surdeanu, R.J. Wijngaarden, J. Einfeld, R. Wördenweber and R. Griessen, Europhysics Lett. **54**, 682 (2001).
- ²⁰ P. Leiderer, J. Boneberg, P. Brüll, V. Bujok, and S. Herminghaus, Phys. Rev. Lett. **71**, 2646 (1993).
- ²¹ Small imperfections as indentations in the sample's border lead to a deformation of the screening currents that can trigger or promote dendrite nucleation. In our particular case one of the substrate edges was deliberately cut to create a rough sample edge, however no clear evidence of a higher dendrite density was detected.
- ²² L. D. Cooley and A. M. Grishin, Phys. Rev. Lett. **74**, 2788 (1995).
- ²³ V. V. Moshchalkov, M. Baert, V. V. Metlushko, E. Rosseel, M. J. Van Bael, K. Temst, R. Jonckheere, and Y. Bruynseraede, Phys. Rev. B **57**, 3615 (1998).
- ²⁴ F. L. Barkov, D. V. Shantsev, T. H. Johansen, P. E. Goa, W. N. Kang, H. J. Kim, E. M. Choi, S. I. Lee, Phys. Rev. B **67**, 064513 (2003).
- ²⁵ M. S. Welling, R. J. Westerwaal, W. Lohstroh, and R. J. Wijngaarden, Physica C **411**, 11 (2004).
- ²⁶ E. Altshuler and T. H. Johansen, Rev. Mod. Phys. **76**, 471 (2004) and references therein.
- ²⁷ H. A. Radovan and R. J. Zieve, Phys. Rev. B **68**, 224509 (2003).

- ²⁸ We did not perform a finite size scale analysis because the anisotropic shape of avalanches (elongated in one direction) introduces artifacts in the size distribution when selecting a system length, L , smaller than the size of the sample.
- ²⁹ C.M.Aegerter, M.S.Welling and R.J.Wijngaarden, *Europhys. Lett.* **65**, 753 (2004).

V. FIGURE CAPTIONS

FIG. 1: MO images of the Pb sample AD75 with antidots showing different types of flux penetration: (a) finger-like dendritic penetration at $\mu_0 H = 1.2$ mT and $T = 4.5$ K and (b) $\mu_0 H = 1.2$ mT and $T = 5.5$ K, (c) tree-like dendritic outburst coexisting with smooth flux penetration at $\mu_0 H = 1.5$ mT and $T = 6$ K, and (d) smooth profile at $\mu_0 H = 1.5$ mT and $T = 6.5$ K. A saw-tooth-like magnetic wall domain artifact from the magneto-optical garnet is observed in the bottom part of the images. (e) and (f) MO images of a Pb plain film at $T = 2.5$ K for $\mu_0 H = 0.4$ mT and $\mu_0 H = 1.2$ mT respectively. The scale bar in each figure corresponds to 0.5 mm.

FIG. 2: Phase boundary lines, $H^*(T)$, separating dendritic from smooth penetration for different samples. Open symbols correspond to ac-susceptibility measurements¹² while filled symbols are values obtained by MO imaging. (a) Results for samples with antidots AD65 and AD75. (b) Comparison between a plain film (PF15) and a sample with antidots (AD15) (see Table I).

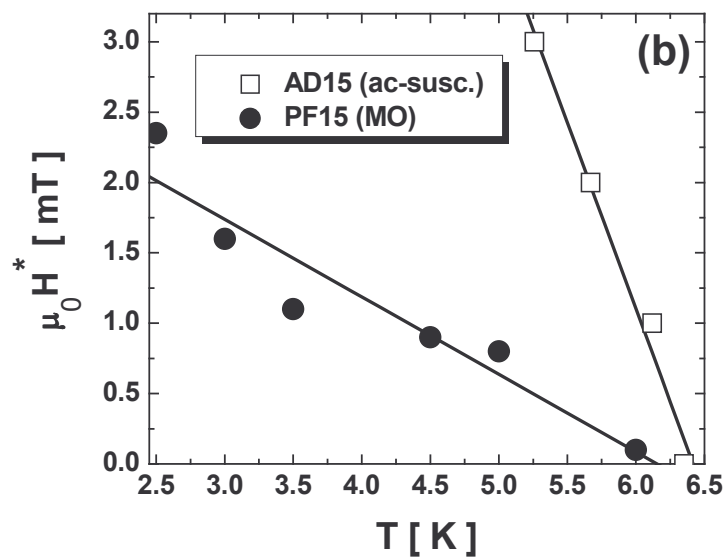
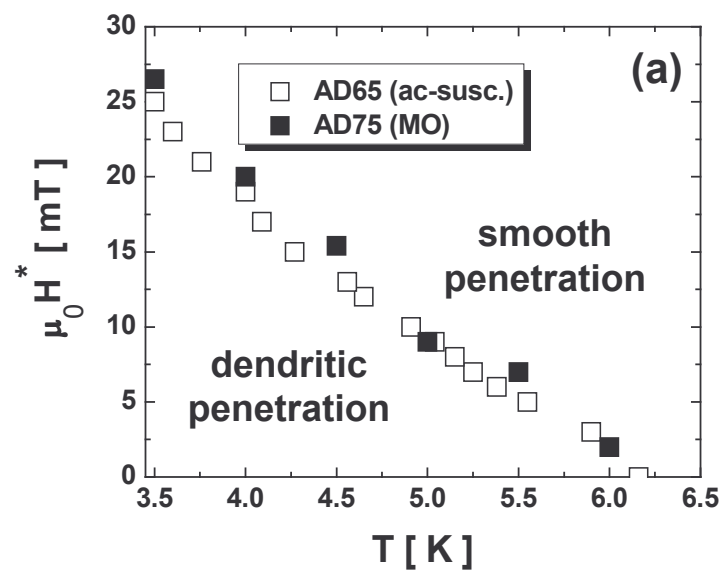
FIG. 3: (a) Three-dimensional plot of magnetic field near the edge of the sample (AD75) with antidots at $T = 4$ K and $\mu_0 H = 1.8$ mT. (b) Profiles of magnetic field along a dendrite indicated by A-A' in (a) for different applied fields. (c) Sequence of magnetic field profiles along the line B-B' in (a) (transverse to the dendrites). For clarity the curves are displaced by 1.5 mT along the vertical axis. The difference in external field between each consecutive profile is 0.2 mT.

FIG. 4: Avalanches as a function of applied field for sample AD75. (a) Total magnetic flux, Φ_T , (b) area of the sample covered by avalanches, A_T and (c) average size of avalanches, $\langle \Phi \rangle$, at each field step as a function of H for different temperatures.

FIG. 5: Log-log plot of the distribution of avalanche sizes for sample AD75 at different temperatures. The size of an avalanche is given by the moved flux Φ . The straight solid lines are linear fits, yielding a power-law exponent $\tau = 0.9(1)$.

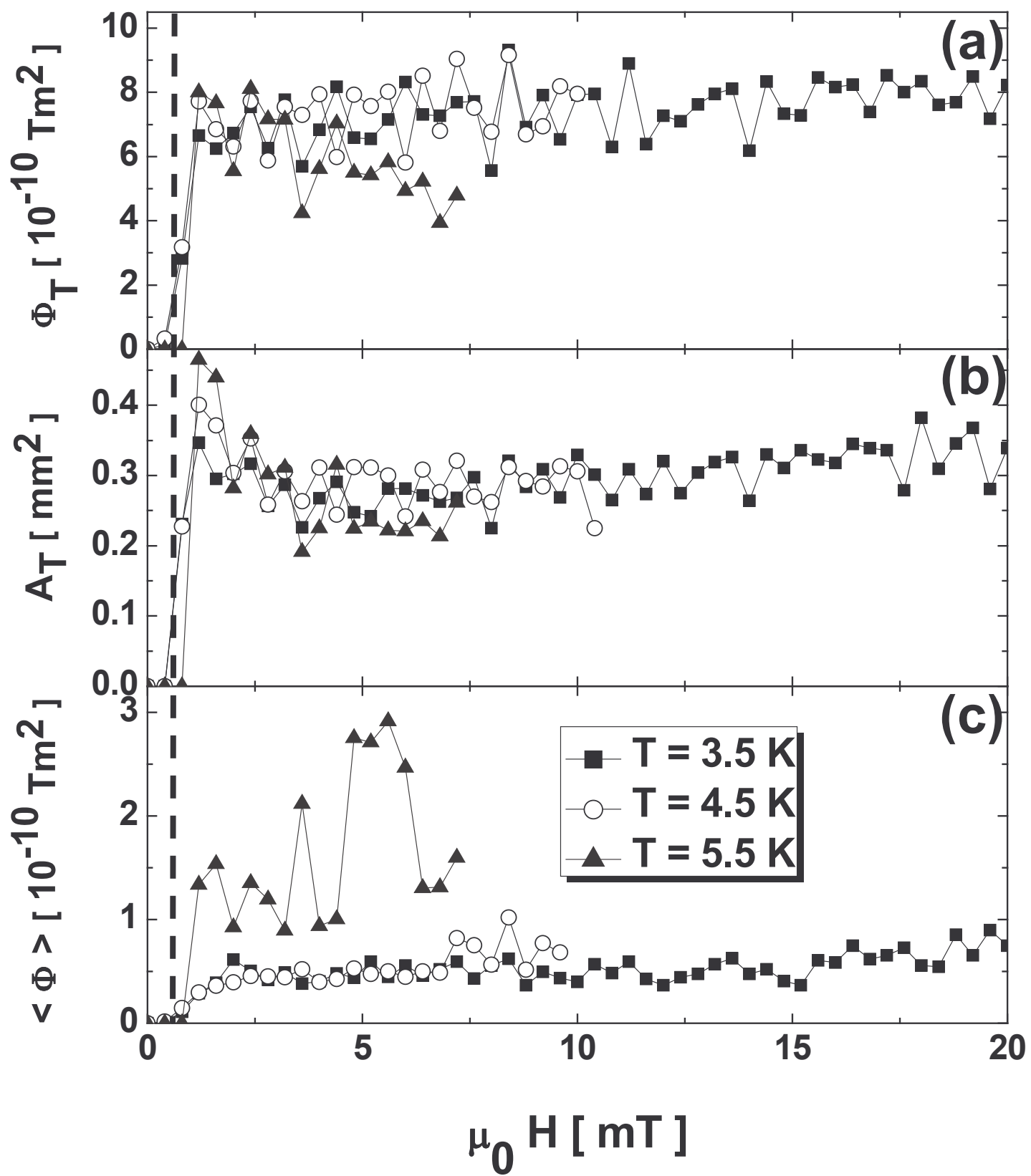
This figure "Fig1.jpg" is available in "jpg" format from:

<http://arxiv.org/ps/cond-mat/0409391v1>



This figure "Fig3.jpg" is available in "jpg" format from:

<http://arxiv.org/ps/cond-mat/0409391v1>



This figure "Fig5.jpg" is available in "jpg" format from:

<http://arxiv.org/ps/cond-mat/0409391v1>